Investigating Interfacial Chemistry for Pre-passivated Lithium-ion Battery Electrodes Employing Non-flammable Methyl(2,2,2-trifluoroethyl) carbonate Electrolytes

Lasse Dettmann[1], Florian Gebert[1] and Andrew J. Naylor[1*]

[1] *Department of Chemistry-Ångström Laboratory, Uppsala University, SE-751 21, Uppsala, Sweden*

[*] *Corresponding author: andy.naylor@kemi.uu.se*

Supplementary Information

Flammability Tests

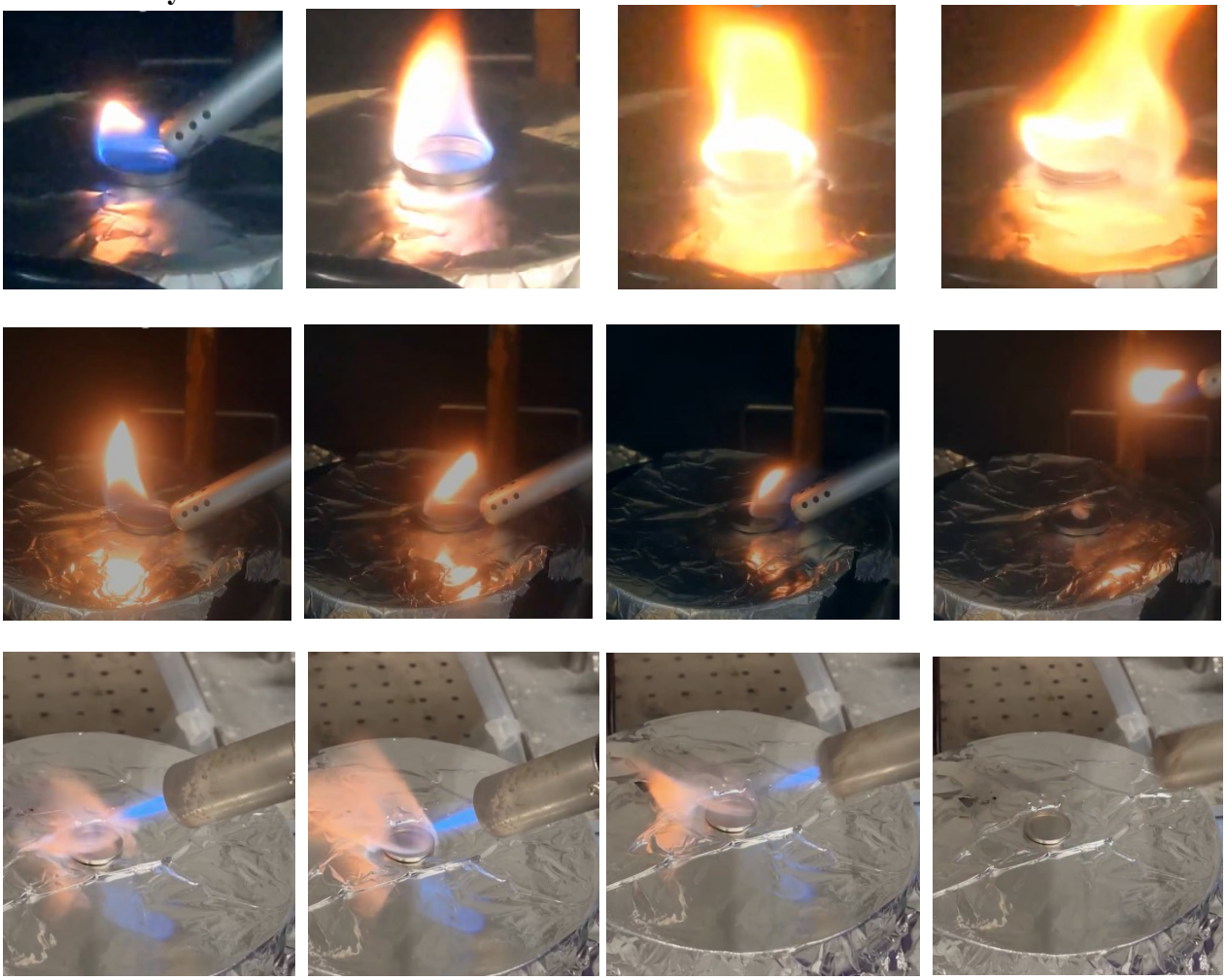

Figure S1. Flammability comparison of three Li-ion battery electrolytes. **Top row:** LP57 (1 M $LiPF_6$ in EC/EMC, 3:7 v/v) during ignition and burning. After ignition, the electrolyte sustains a stable flame with increasing intensity from left to right, resulting in a long self-extinguishing time of 76 ± 1 s g^{-1}. **Middle row:** Pure FEMC-based electrolyte (1 M $LiPF_6$ in methyl(2,2,2-trifluoroethyl) carbonate). Following ignition, the flame is rapidly quenched, as illustrated by the sequence from left to right, indicating a very short self-extinguishing time and demonstrating the non-flammable behaviour of the FEMC solvent. **Bottom row:** FEMC containing 5 vol% LP57. Similar to the pure FEMC-based electrolyte, ignition leads to rapid flame quenching, demonstrating a very short self-extinguishing time and confirming that the electrolyte remains non-flammable even in the presence of 5 vol% LP57.

Galvanostatic Cycling

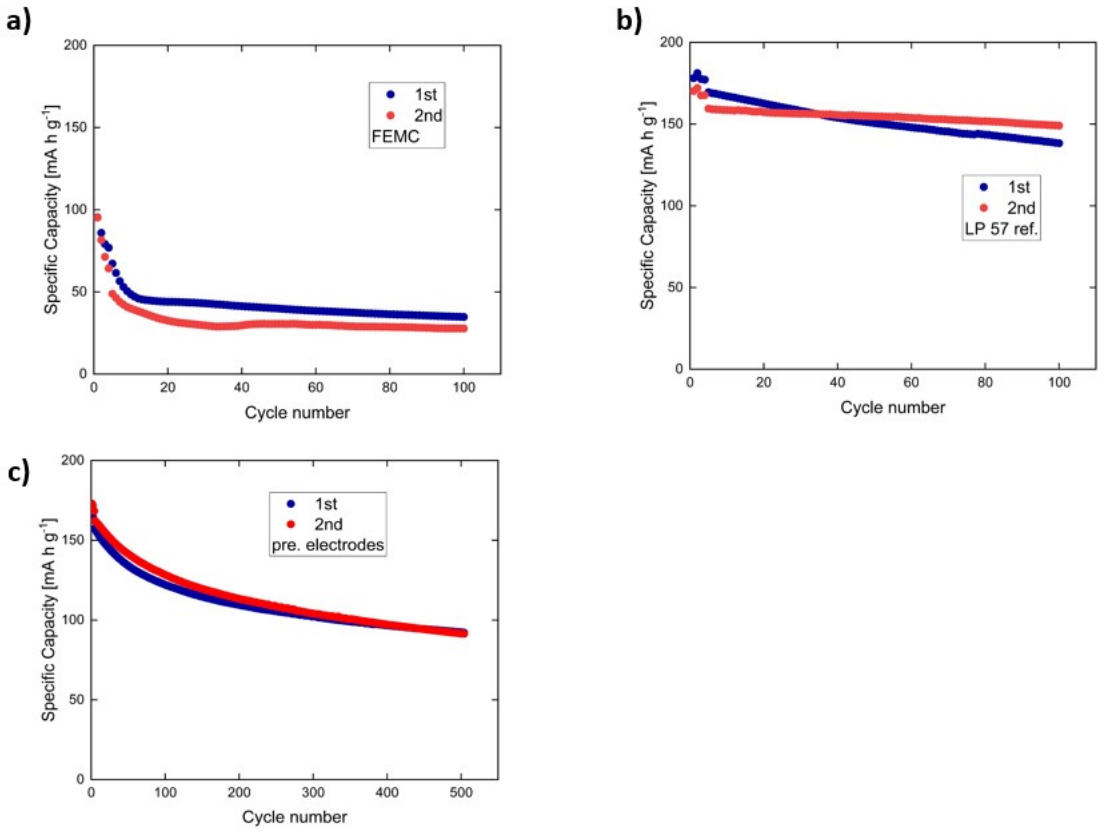

Figure S2. Overlay of galvanostatic cycling data demonstrating the reproducibility of the results shown in Figure 1a and 1b of the main manuscript. Each color represents an individual cell. **a)** Cycling performance in pure FEMC electrolyte (corresponding to the red curve in Figure 1a), **b)** Cycling performance in LP57 benchmark electrolyte (blue curve in Figure 1a), **c)** Cycling performance of FEMC with pre-passivated electrodes in LP57 (green curve in Figure 1a and b).

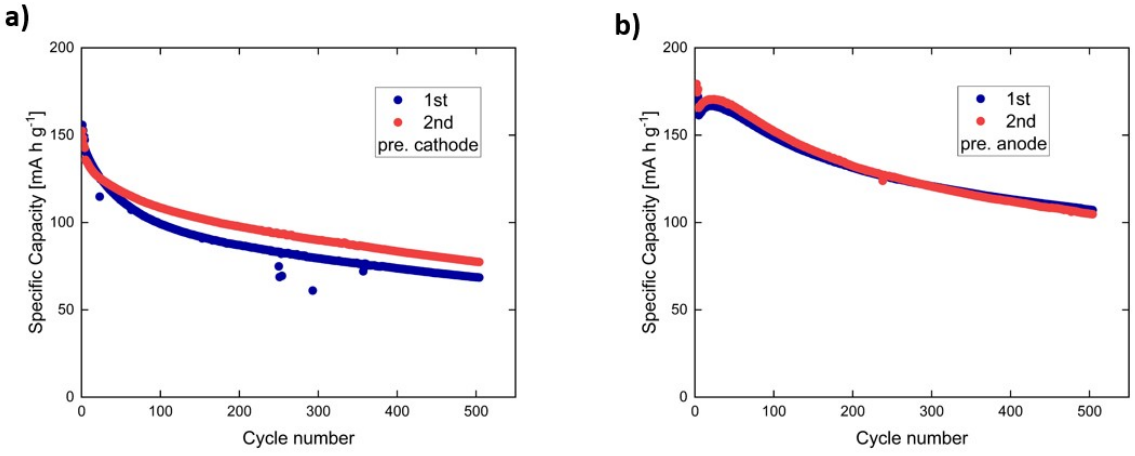

Figure S3. Overlay of galvanostatic cycling data demonstrating the reproducibility of the results shown in Figure 1b of the main manuscript. Each color represents an individual cell. **a)** Cycling performance in FEMC with a pre-passivated cathode in LP57 electrolyte (corresponding to the purple curve in Figure 1b), **b)** Cycling performance in FEMC with a pre-passivated anode in LP57 electrolyte (corresponding to the black curve in Figure 1b).

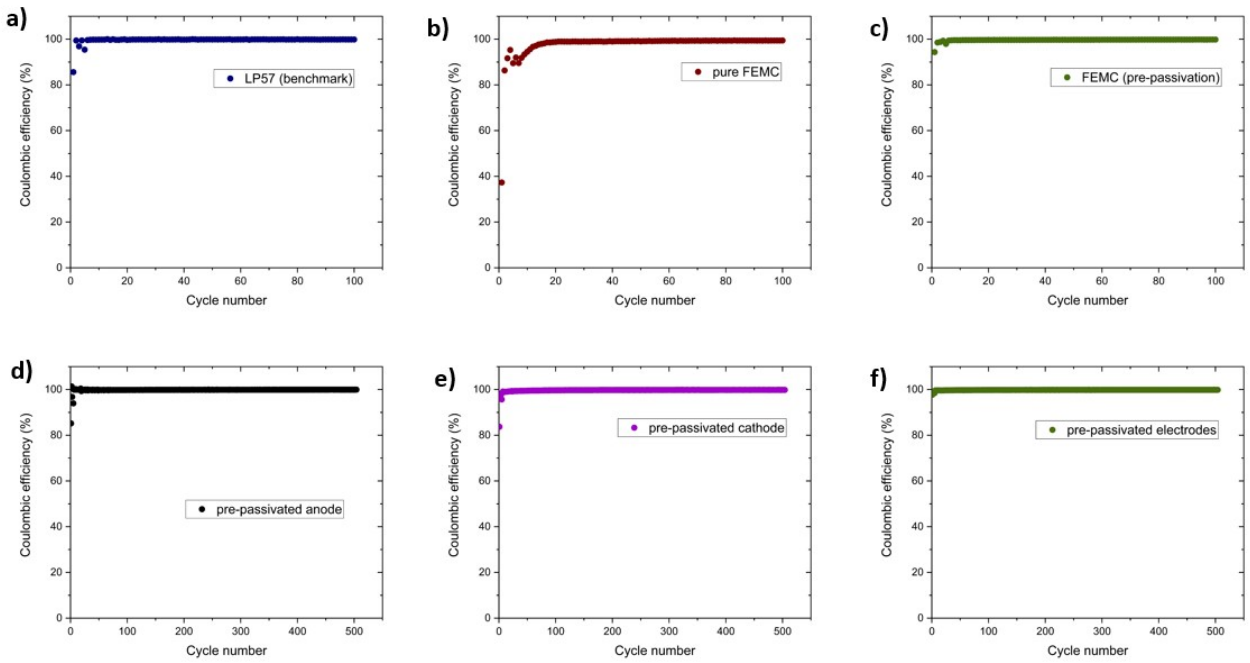

Figure S4. Coulombic efficiency (%) vs. cycle number plots corresponding to the cycling data shown in Figure 1a and 1b of the main manuscript. These plots show the charge/discharge efficiency for each configuration. **a)** Cycling performance in LP57 electrolyte (corresponding to the blue curve in Figure 1a), **b)** Cycling performance in pure FEMC electrolyte (corresponding to the red curve in Figure 1a), **c)** Cycling performance in FEMC with pre-passivated electrodes in LP57 electrolyte (corresponding to the green curve in Figure 1a), **d)** Cycling performance in FEMC with a pre-passivated anode in LP57 electrolyte (corresponding to the black curve in Figure 1b), **e)** Cycling performance in FEMC with a pre-passivated cathode in LP57 electrolyte (corresponding to the purple curve in Figure 1b), **f)** Cycling performance in FEMC with both electrodes pre-passivated in LP57 electrolyte (corresponding to the green curve in Figure 1b).

X-ray photoelectron spectroscopy

Figures S5–S12 present the C 1s, F 1s, O 1s, and Li 1s XPS spectra acquired at varying probing depths for the two partial pre-passivation configurations: (i) cathode-only pre-passivation with a pristine anode and (ii) anode-only pre-passivation with a pristine cathode. These depth-resolved spectra allow comparison of the resulting SEI compositions and their stability, in direct support of the discussion in the main text.

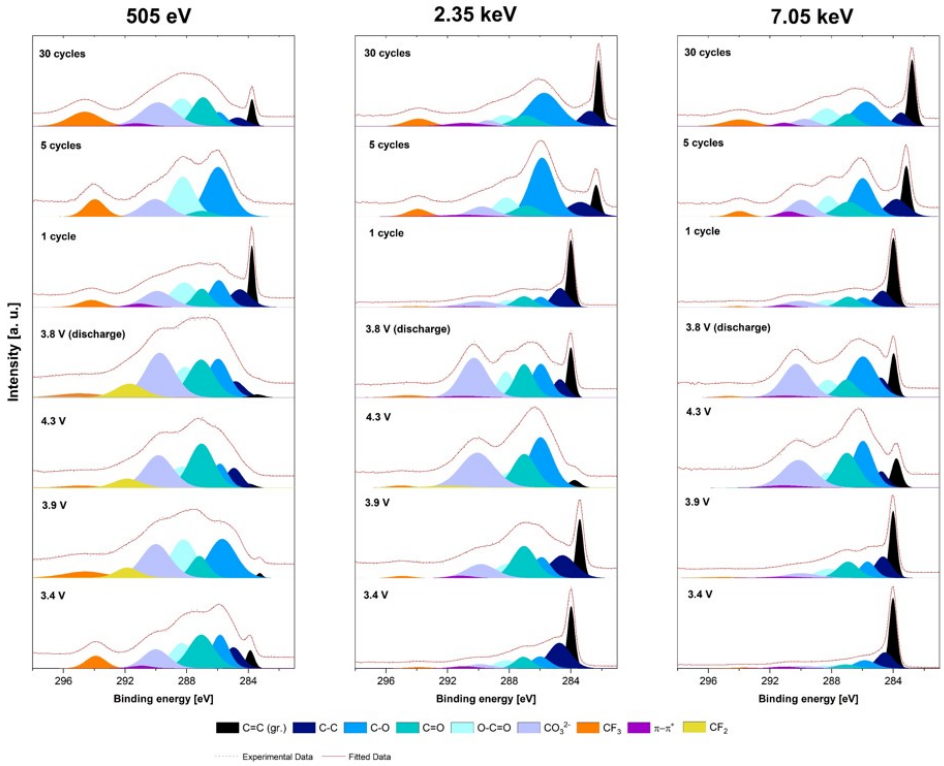

Figure S5. C 1s XPS spectra acquired at excitation energies of 505 eV (left), 2.35 keV (center), and 7.05 keV (right) showing the SEI composition on graphite electrodes from NMC622 // graphite cells aged to different states of charge and for different amount of cycles at C/2 in FEMC. The cathode was pre-passivated and the anode was left pristine for all cells before aging in FEMC.

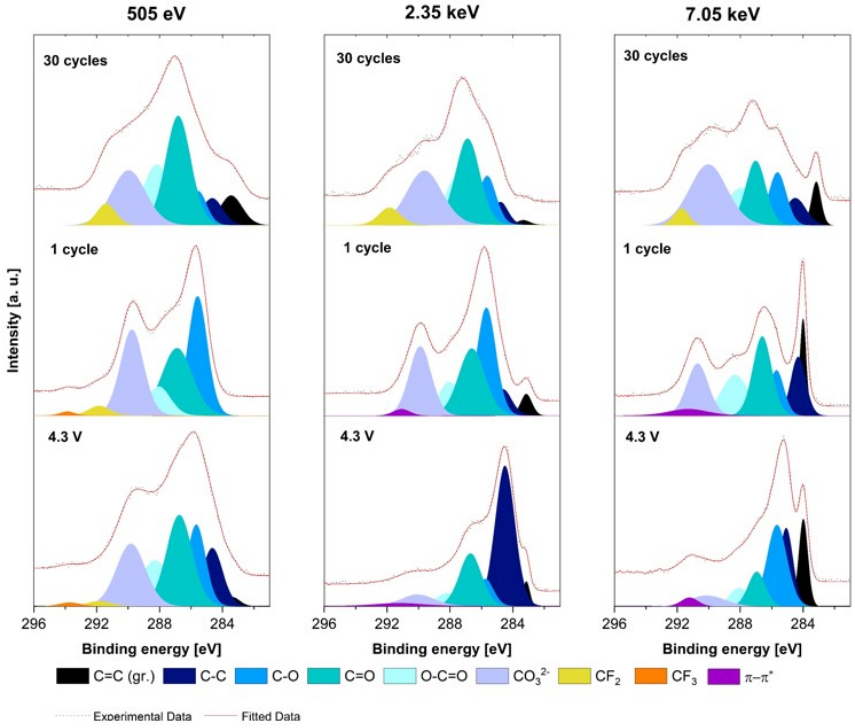

Figure S6. C 1s XPS spectra acquired at excitation energies of 505 eV (left), 2.35 keV (center), and 7.05 keV (right) showing the SEI composition on graphite electrodes from NMC622 // graphite cells aged to different states of charge and for different amount of cycles at C/2 in FEMC. The anode was pre-passivated and the cathode was left pristine for all cells before aging in FEMC.

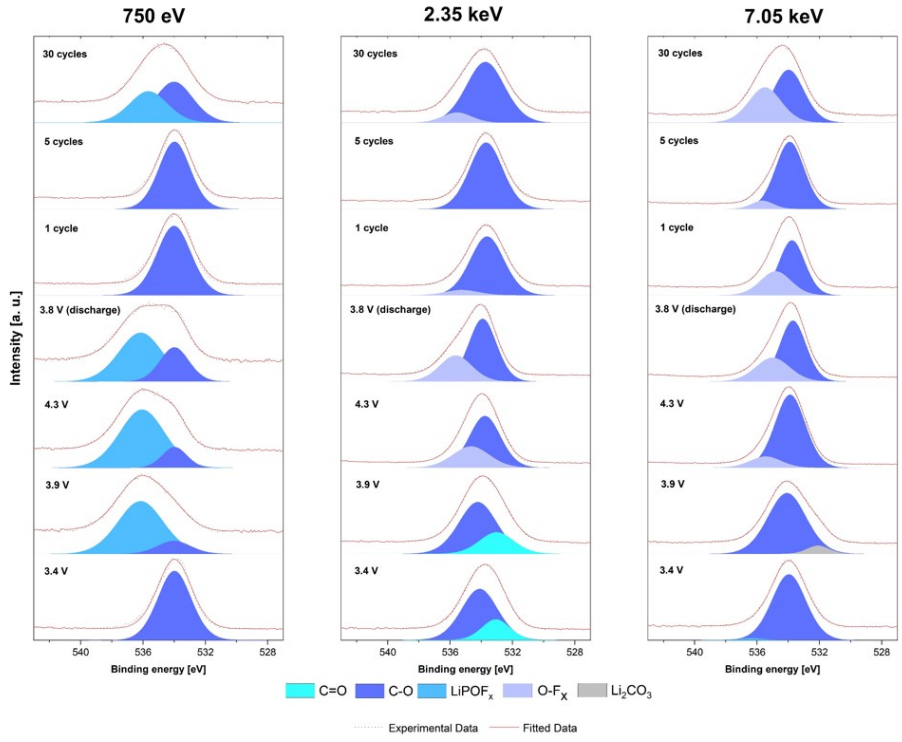

Figure S7. O 1s XPS spectra acquired at excitation energies of 910 eV (left), 2.35 keV (center), and 7.05 keV (right) showing the SEI composition on graphite electrodes from NMC622 // graphite cells aged to different states of charge and for different amount of cycles at

C/2 in FEMC. The cathode was pre-passivated and the anode was left pristine for all cells before aging in FEMC.

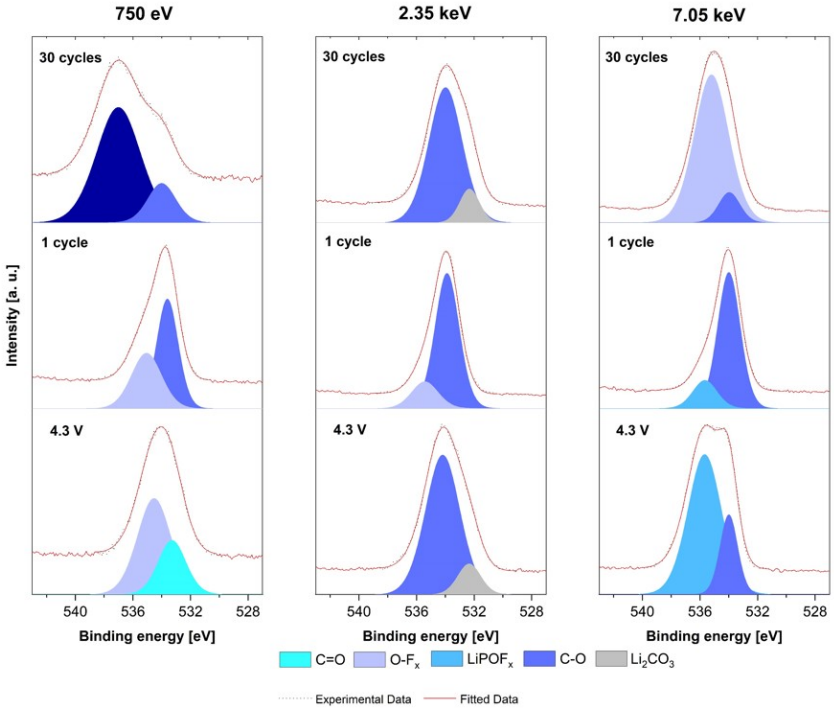

Figure S8. O 1s XPS spectra acquired at excitation energies of 750 eV (left), 2.35 keV (center), and 7.05 keV (right) showing the SEI composition on graphite electrodes from NMC622 // graphite cells aged to different states of charge and for different amount of cycles at C/2 in FEMC. The anode was pre-passivated and the cathode was left pristine for all cells before aging in FEMC.

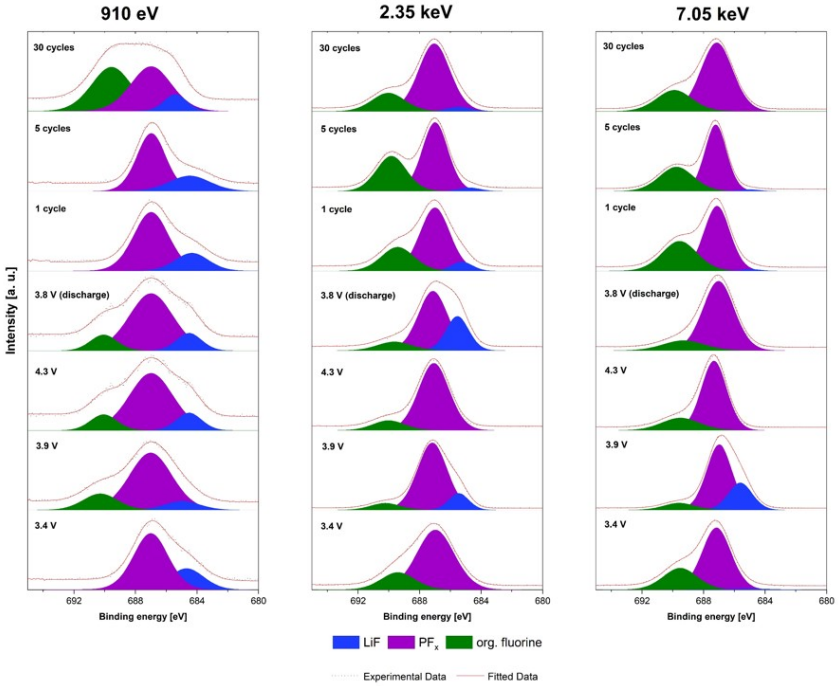

Figure S9. F 1s XPS spectra acquired at excitation energies of 910 eV (left), 2.35 keV (center), and 7.05 keV (right) showing the SEI composition on graphite electrodes from NMC622 // graphite cells aged to different states of charge and for different amount of cycles at

C/2 in FEMC. The cathode was pre-passivated and the anode was left pristine for all cells before aging in FEMC.

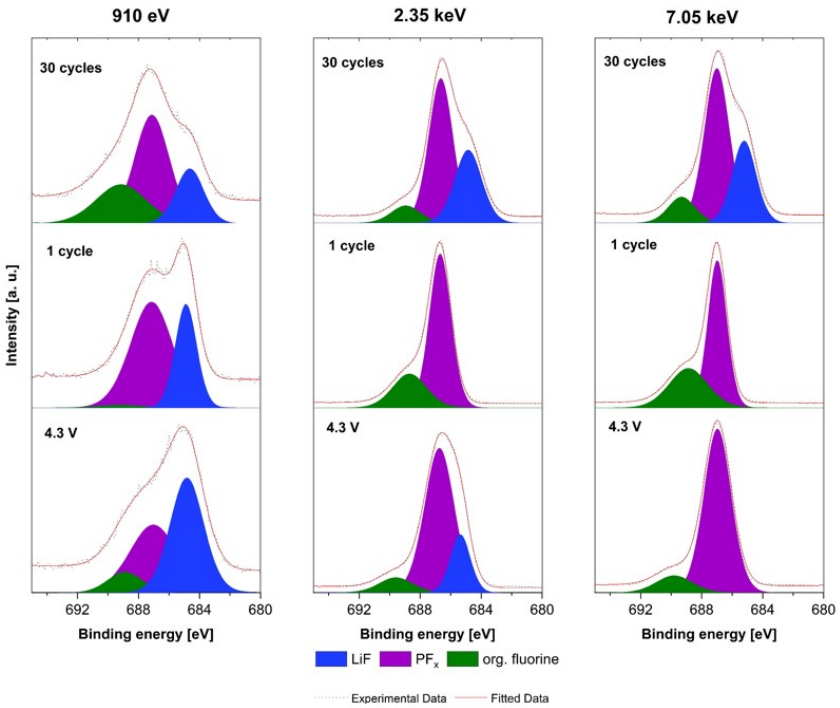

Figure S10. F 1s XPS spectra acquired at excitation energies of 910 eV (left), 2.35 keV (center), and 7.05 keV (right) showing the SEI composition on graphite electrodes from NMC622 // graphite cells aged to different states of charge and for different amount of cycles at C/2 in FEMC. The anode was pre-passivated and the cathode was left pristine for all cells before aging in FEMC.

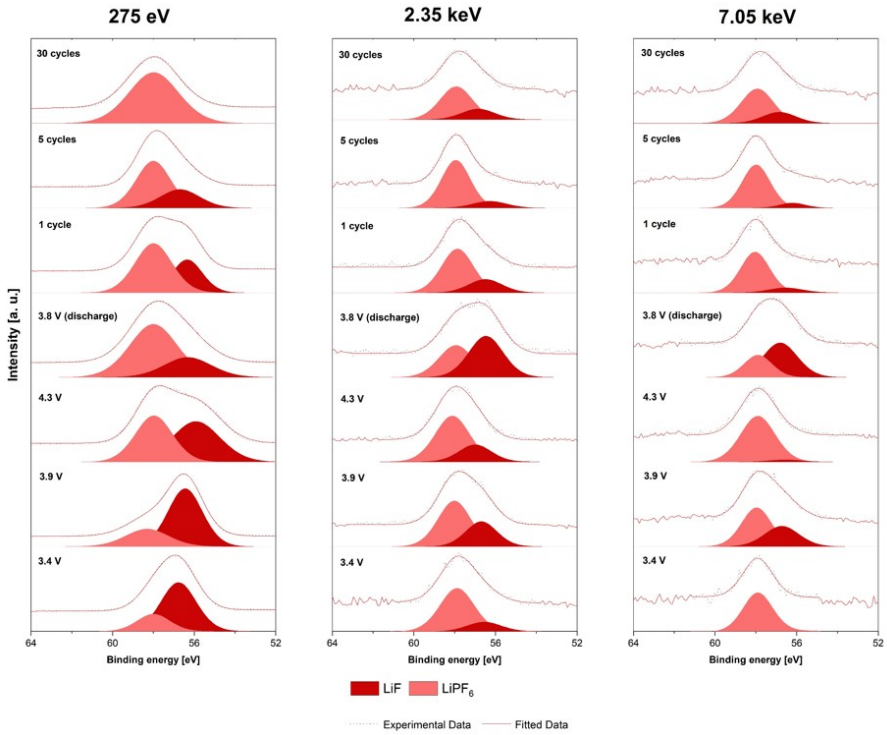

Figure S11. Li 1s XPS spectra acquired at excitation energies of 275 eV (left), 2.35 keV (center), and 7.05 keV (right) showing the SEI

composition on graphite electrodes from NMC622 // graphite cells aged to different states of charge and for different amount of cycles at C/2 in FEMC. The cathode was pre-passivated and the anode was left pristine for all cells before aging in FEMC.

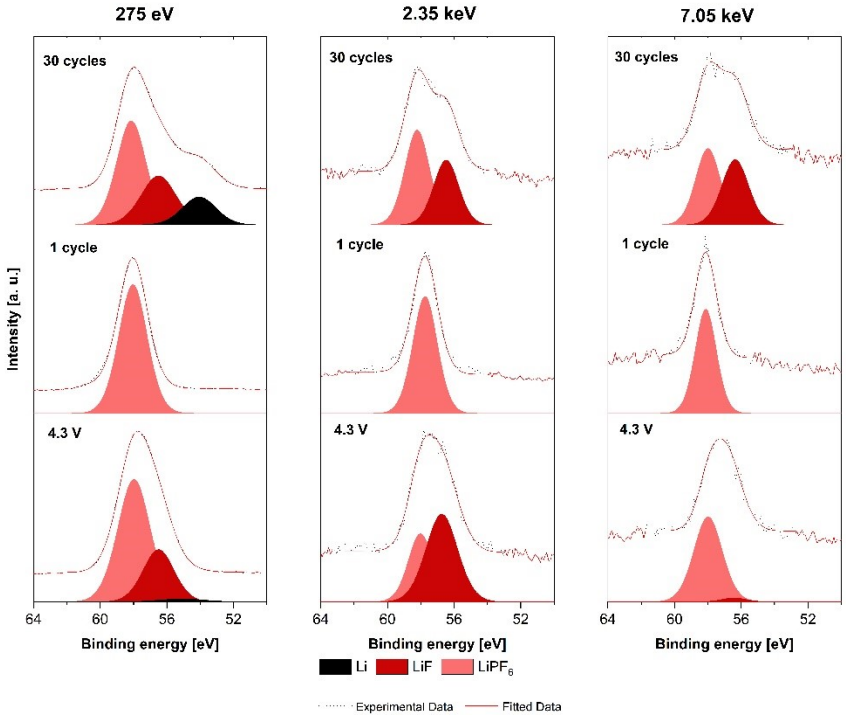

Figure S12. Li 1s XPS spectra acquired at excitation energies of 275 eV (left), 2.35 keV (center), and 7.05 keV (right) showing the SEI composition on graphite electrodes from NMC622 // graphite cells aged to different states of charge and for different amount of cycles at C/2 in FEMC. The anode was pre-passivated and the cathode was left pristine for all cells before aging in FEMC.

Galvanostatic Cycling

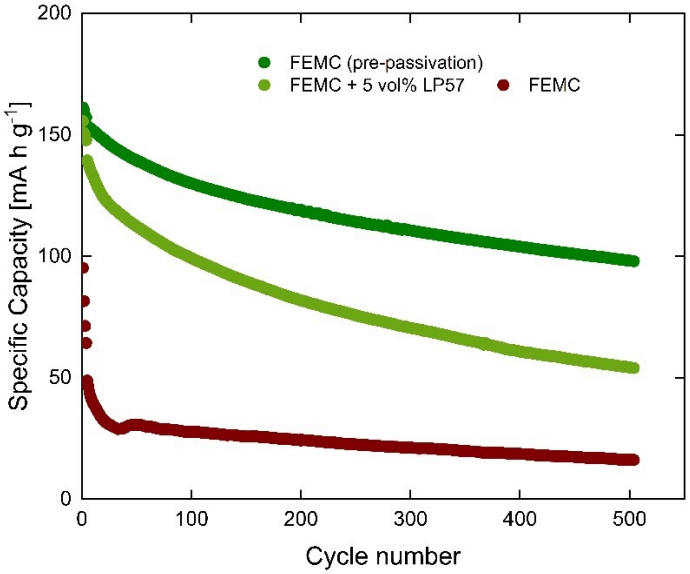

Figure S13. Galvanostatic cycling performance under different FEMC-based electrolyte and pre-passivation conditions. Comparison of cells employing FEMC with pre-passivated electrodes (dark green), FEMC containing 5 vol% LP57 (light green), and pure FEMC without pre-passivation (red). Despite the presence of 5 vol% residual LP57 in the FEMC electrolyte, the corresponding cells exhibit inferior cycling stability compared to FEMC with pre-passivated electrodes. This highlights that the observed performance enhancement originates from the pre-passivation procedure rather than from residual LP57 components in the FEMC electrolyte.

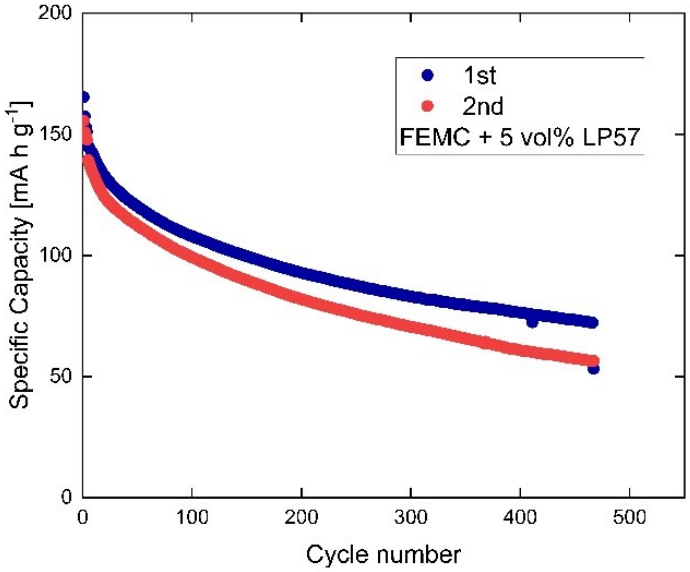

Figure S14. Overlay of galvanostatic cycling data demonstrating the reproducibility of the results shown in Figure S13. Each color represents an individual cell. Cycling was performed in FEMC containing 5 vol% LP57, corresponding to the light green curve in Figure S13.